Available online at www.sciencedirect.com

SCIENCE DIRECT

JOURNAL OF CONSTRUCTIONAL STEEL RESEARCH

ELSEVIER Journal of Constructional Steel Research 60 (2004) 601–620

www.elsevier.com/locate/jcsr

On the rotation capacity of moment connections

Darko Beg [a,*], Erik Zupančič [a], Ioannis Vayas [b]

[a] Faculty of Civil and Geodetic Engineering, University of Ljubljana, Jamova 2, 1000 Ljubljana, Slovenia
[b] School of Civil Engineering, National Technical University of Athens, Patission str. 42, 10682 Athens, Greece

Abstract

The paper presents an analytical method for the determination of the rotation capacity of moment connections, based on the component method from prEN 1993-1-8. From test results and numerical simulations, simple analytical expressions for the deformation capacity of the components are derived. These values are subsequently used for the determination of the rotation capacity of the complete joint. Comparisons with tests on whole joints indicate a good agreement between analytical and experimental results. The method is fully consistent with the present rules of prEN 1993-1-8 and extends them to the numerical estimation of the rotation capacity.

Keywords: Steel structures; Moment connections; Joints; Rotation capacity; Component method

1. Introduction

Three basic parameters describe the behaviour of connections: strength, stiffness and ductility. In moment resistant connections, the ductility is achieved by a sufficient rotation capacity. Although there do exist well-elaborated methods for determination of the initial stiffness and strength of beam-to-column joints [1,2], there are no generally accepted procedures for the determination of the rotation capacity. Indicatively it may be said that the relevant Eurocode, prEN 1993-1-8 [1]

* Corresponding author. Tel.: +386 1 4768626; fax: +386 1 4768629.
E-mail address: dbeg@fgg.uni-lj.si (D. Beg).

doi:10.1016/S0143-974X(03)00132-9

devotes only one out of 75 pages to the determination of the rotation capacity. The estimation of the rotation capacity is very important in many applications, as e.g. when partial-strength connections are used under seismic conditions or plastically designed frames. It is therefore evident that a simple method for the determination of the rotation capacity for everyday design applications is needed.

This paper presents an analytical method for the determination of the rotation capacity of moment connections. The intention is not to develop completely new rules, but to upgrade the existing procedure of prEN 1993-1-8 [1], to include the determination of the rotation capacity. For this reason, the component method is used and the initial stiffness and the strength, which are needed in the process of the calculation of the rotation capacity, are determined according to [1]. The main task here is to determine the deformation capacities of the basic components of a joint.

The deformation capacity of components has been studied by several researchers [3–7]. Faella et al. [8] carried out tests on T-stubs and derived analytical expressions for the deformation capacity of this component. Kuhlmann and Kuhnemund [9] performed tests on the column web subjected to transverse compression at different levels of compression axial force in the column. Some authors have tried to extract the information of the behaviour of single components from the tests on a whole joint. Bose et al. [10,11] determined only the strength of the most important components, while da Silva et al. [12] tried to determine all three important parameters, stiffness, strength and deformation capacity, at different levels of axial force in a beam.

Based on the test results of other authors and partly on our own tests, combined with FE analysis [13], deformation capacities for all the relevant components are established and presented in Section 2. Single components are then represented by non-linear springs, and appropriately combined in order to determine the rotation capacity of the joint, as shown in Section 3.

2. Deformation capacity of components

2.1. Methods and assumptions

The most common moment connections are end-plate connections, with an extended or flush end-plate, and welded connections (Fig. 1). For these connections, the most important components that may significantly contribute to the rotation capacity of the whole joint are: column web in compression, column web in tension, column web in shear, column flange in bending and end-plate in bending (Fig. 2).

Components related to the column web are relevant only when there are no stiffeners in the column that resist compression, tension or shear forces. The presence of a relevant stiffener eliminates the corresponding component, and its contribution to the rotation capacity of the joint can be therefore neglected. End-plates and column flanges are important only for end-plate connections. Both components act as

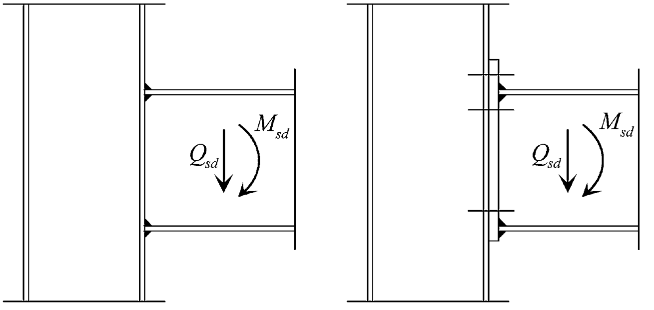

Fig. 1. Typical welded and end-plate bolted connections.

a T-stub, where also the deformation capacity of the bolts in tension is included [14–16].

A simplified force–displacement relationship for each component following the idea of prEN 1993-1-8 can be defined, as shown in Fig. 3. δ_u is the deformation capacity of the component, but there is no indication in the code how to calculate it.

In this paper, the following procedure is used for the determination of deformation capacity, δ_u, of individual components:

- For each component, FE analysis was calibrated against the available test results. During the calibration procedure, an appropriate FE mesh was established. The analysis was made by means of the ABAQUS computer program. The components were modelled by 8- and 20-node 3D solid brick finite elements. Plastic constitutive relations, based on the Mises yield criterion with associated flow rule and isotropic hardening, were used. Where appropriate, initial geometric imperfections for the column webs were introduced. The shape of the imperfections was obtained from the first buckling mode, while the maximum

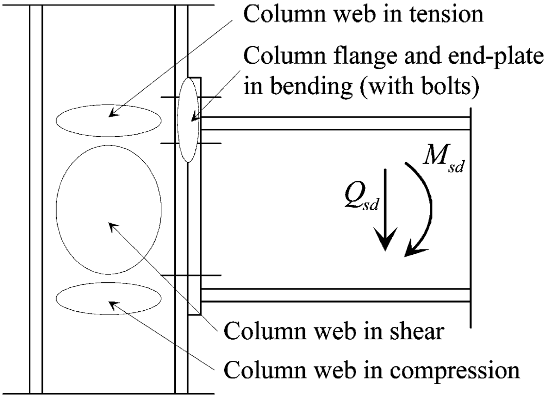

Fig. 2. Components of steel structure connections important for rotation capacity.

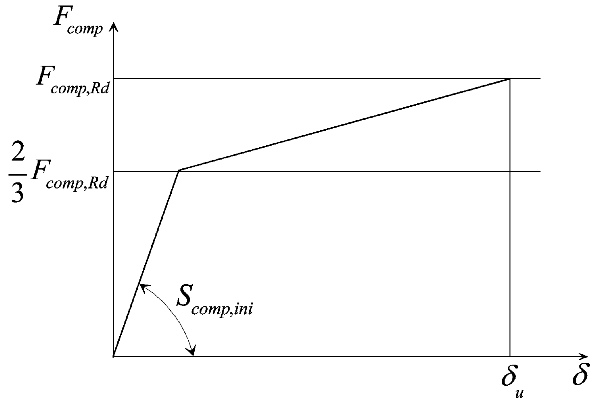

Fig. 3. Simplified force–displacement diagram of components.

amplitude was scaled to an appropriate value. The modelling of the components was done in such a way that the influence of other components on the component under investigation was excluded, as much as possible, in order to prevent the duplication of contributions to the deformation capacity.

- A parametric study of the deformation behaviour of each component was performed by means of FE analysis. The main parameters were the level of the column axial force and the column web slenderness.
- Based on these parametric studies, analytical expressions for δ_u were established.

In order to obtain safe-sided results, displacements corresponding to the maximum resistance were taken as the deformation capacity. In the cases where force–displacement diagrams exhibited a long plastic plateau, the deformation capacity was limited to the values reached at the relevant principal strain of 10% (column web) or 20% (T-stub).

The results of the calibration process are described in detail in Zupančič [13], Vayas et al. [17] and Beg et al. [18], and in this paper only the results of the parametric study are presented.

2.2. Column web in compression

The basic idea of this component is presented in Fig. 4. The transverse compression comes from the compression flanges of the connected beams [19]. Another important load is the axial load in the column.

The test results of Kuhlmann and Kuhnemund [9] were used for the calibration of the numerical model. The authors made a set of tests on HEB 240 profiles acting as the column section. The columns were subjected to axial compression forces of different magnitude and were kept constant during the tests. Point loads were introduced transversally to produce transverse compression in the column web.

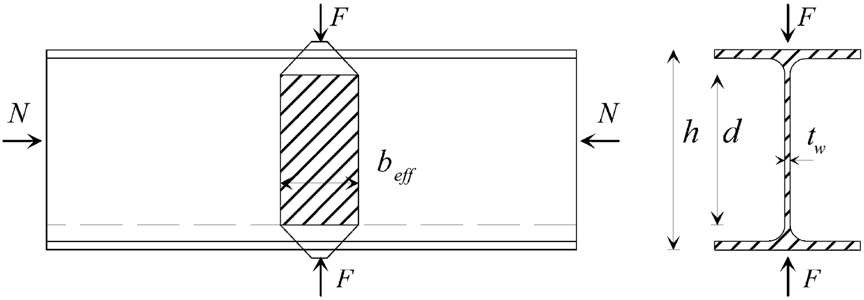

Fig. 4. Geometry of the component column web in compression.

The parametric study for a component column web in compression was performed for a set of profiles with different web slenderness (HEB 100, HEB 240, HEB 400, HEB 500, HEB 600, HEB 700, HEB 1000), each loaded with a range of axial forces, defined as a fraction of axial plastic resistance N_{pl} ($n = N/N_{\mathrm{pl}}$: 0, 0.1, 0.2, 0.3, 0.4, 0.5).

Altogether 42 calculations were done, resulting in a set of deformation capacities δ_{u}. The equivalent ultimate transverse strain in the web can be determined from Eq. (1):

$$\varepsilon_{\mathrm{u}} = \frac{\delta_{\mathrm{u}}}{d}, \tag{1}$$

where d is the depth of the web defined in Fig. 4. ε_{u} can be regarded as a non-dimensional deformation capacity.

The results for ε_{u}, as a function of axial force in the column and the web slenderness, are presented in Fig. 5. The deformation capacity is decreased with the increase of web slenderness, but a constant lower value is reached at higher slenderness. The influence of the axial force is more important at smaller slenderness. Black dots represent the deformation capacities from FE analysis and the three-linear diagrams represent the best fit analytical expressions, given in detail in Vayas et al. [17].

2.3. Column web in tension

There were no test results available for this component. In this case, the mechanical behaviour is relatively simple. The analytical expression for the deformation capacity is first derived and subsequently tested with the results of the numerical simulation.

Deformation capacity, δ_{u}, can be expressed as follows:

$$\delta_{\mathrm{u}} = \varepsilon_{\mathrm{u}} \cdot d \tag{2}$$

where ε_{u} is a transverse strain corresponding to the ultimate resistance of the web

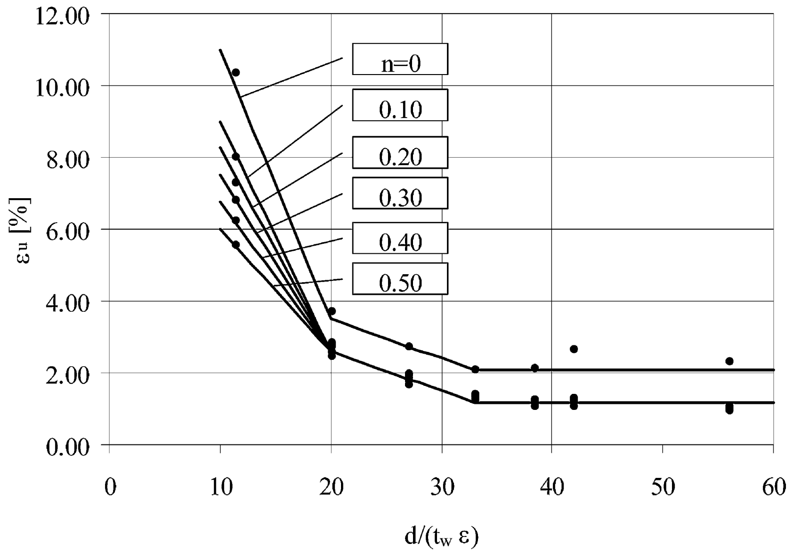

Fig. 5. ε_u as a function of axial force n and web slenderness $d/(t_w \cdot \varepsilon)$, $\varepsilon = \sqrt{235/f_y}$.

and d is defined in Fig. 6. The yield criterion at biaxial stress conditions in the web can be written as:

$$f_y \geq \sqrt{\sigma_x^2 + \sigma_y^2 + \sigma_x \cdot \sigma_y}, \tag{3}$$

where σ_x is the absolute value of the compression stress, resulting from the axial force, and σ_y is the transverse tension stress.

With $n = \sigma_x/f_y$, Eq. (3) can be rewritten as:

$$\left(\frac{\sigma_y}{f_y}\right)^2 + n \cdot \left(\frac{\sigma_y}{f_y}\right) + n^2 - 1 \leq 0. \tag{4}$$

and solved for σ_y/f_y. For positive values, that are only reasonable, the solution is:

$$\left(\frac{\sigma_y}{f_y}\right) \leq \left(\frac{\sqrt{4 - 3 \cdot n^2} - n}{2}\right) = r. \tag{5}$$

The web resistance, in terms of stresses σ_{yu}, is obtained when the equality sign is set in expression (5). The right-hand term r expresses the influence of a compressive axial force in a non-dimensional form:

$$\sigma_{yu} = f_y \cdot r. \tag{6}$$

A similar expression can be used for the ultimate transverse strain ε_u:

$$\varepsilon_u = \varepsilon_0 \cdot r \tag{7}$$

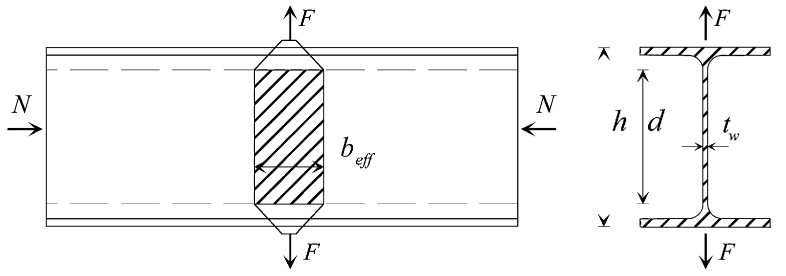

Fig. 6. Geometry of the component column web in tension.

where ε_0 is the ultimate transverse strain in the case when no axial force is present. It is set to $\varepsilon_0 = 0.10$.

The analogy of Eqs. (6) and (7) is not complete and, as will be presented below, better results are obtained when the square of r is used in Eq. (7). Accordingly:

$$\varepsilon_u = \varepsilon_0 \cdot r^2 = 0.1 \cdot \left(\frac{\sqrt{4 - 3 \cdot n^2} - n}{2} \right)^2. \quad (8)$$

This assumption is examined by means of a numerical simulation. The same numerical model as in Section 2.2 was used with the difference that transverse tension, instead of compression, was applied. The numerical analysis was done for HEB 500 profiles, loaded at different levels of axial force. Force–displacement diagrams are shown in Fig. 7. Displacements δ represent the increase of distance between the flanges at the transverse tension.

Black dots represent deformation capacity δ_u, calculated with expression (8), and crosses the, somewhat, larger δ_u, calculated using Eq. (7) instead of Eq. (8). Ultimate strength and deformation capacity decrease with the increase of axial force. At that point, equivalent strain never exceeds the limiting value 0.1. This means that on the long plateau of the force–displacement diagrams, the analytical expression for the deformation capacity gives safe-sided values.

2.4. Web in shear

The component column web in shear, shown in Fig. 8, generally exhibits very ductile behaviour and can significantly contribute to the rotation capacity of joints. The tests of Dubina et al. [20] were selected for the calibration of the numerical analysis.

The numerical parametric study was performed in order to obtain the deformation capacity of the web in shear. Five cross-sections were selected with different web slenderness (HEB 100, HEB 200, HEB 400, HEB 600 and HEB 1000) and loaded with six different axial forces ($n = 0$, 0.1, 0.2, 0.3, 0.4, 0.5).

Typical results for HEB 400 are shown in Fig. 9, where diagrams of transverse force–average rotation γ of the web panel are plotted for different levels of axial

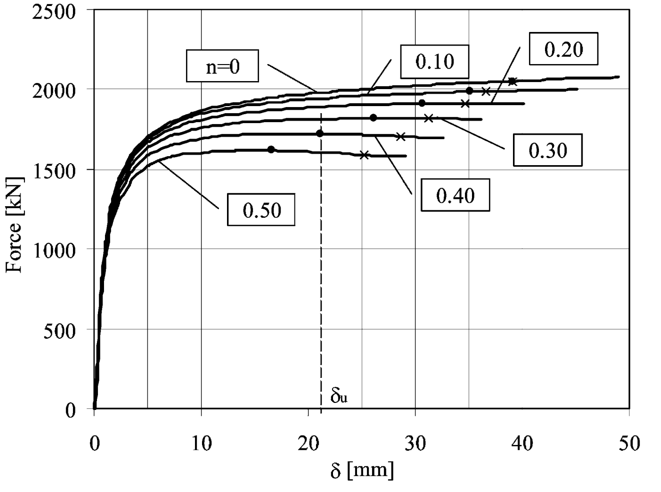

Fig. 7. Results of numerical simulation (column web in tension).

force. Black dots indicate the maximum strength and the corresponding characteristic deformation capacity, measured with panel rotation γ_u.

These ultimate rotations are plotted in Fig. 10, in relation to web depth-to-thickness ratio and the level of the axial force. The positions of dots on the plateau of diagrams in Fig. 9 were slightly rearranged regarding the maximum strength, to obtain perfect linear relationship between ultimate rotation and the web slenderness for each level of axial force. The deformation capacity is not affected much by

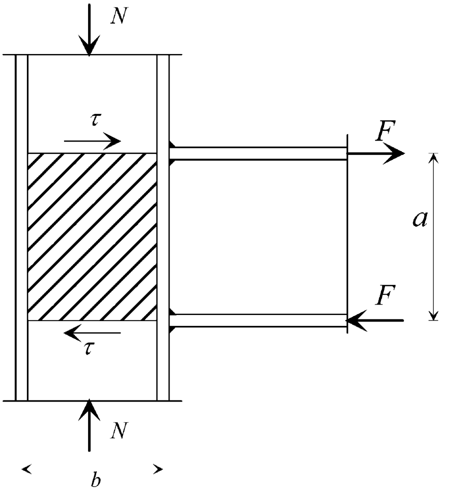

Fig. 8. Component column web in shear.

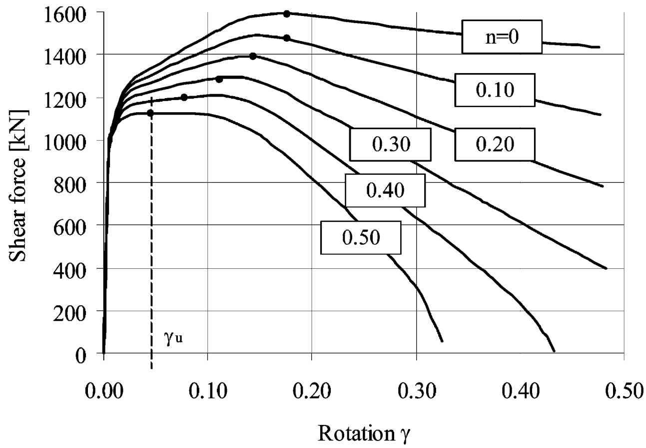

Fig. 9. Diagram shear force–rotation of the panel γ (numerical simulation—HEB 400).

this correction, and is anyway on the safe side. As expected, again the deformation capacity decreases with the increase of web slenderness and axial force, but the relationship is now linear.

2.5. Column flange and end-plate in bending

Of all components under consideration, the T-stub behaviour of column flanges and end-plates is the most complex. Besides bending of the steel plates, the deformations of bolts, nuts and washers are also involved. Different collapse modes are possible and prEN 1993-1-8 [1] distinguishes three collapse modes. Faella et al. [8]

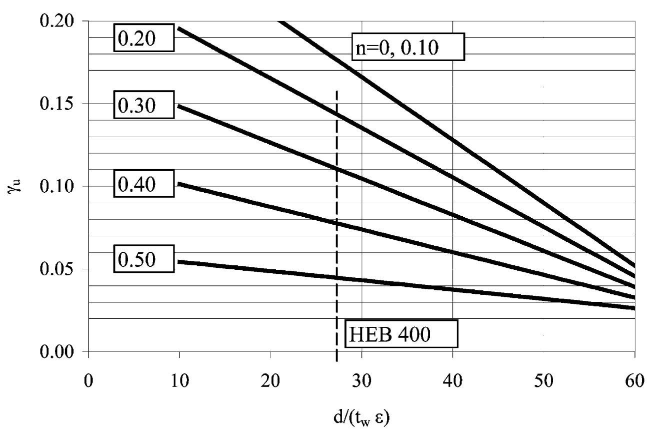

Fig. 10. Ultimate shear strain γ_u.

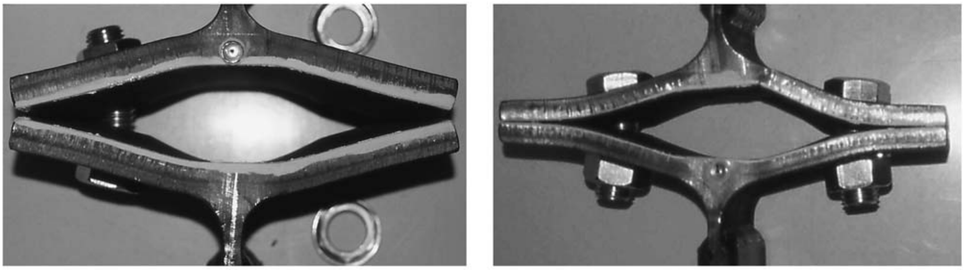

Test specimen 1.1 (HEB 200) Test specimen 2.1 (HEA 260)

Fig. 11. Photos of test specimens after the tests.

proposed an analytical expression for the T-stub deformation capacity, based on own tests, which gives reasonable results but is rather complicated for use.

For this component, simple analytical expressions for all three modes were derived based on four of our own tests and appropriate numerical simulation. Two T-stub assemblies were made with HEB 200 profiles and the other two with HEB 240 profiles. Bolts M20 8.8 and M24 8.8 were used, respectively. Fig. 11 shows test specimens 1.1 and 2.1 after the test. Fig. 12 shows the FE mesh used for the numerical simulations of groups 1 and 2 of specimens.

The comparison between test results and numerical simulations is shown in Fig. 13. It may be seen that a good agreement was achieved. HEB 200 test specimens failed in Mode 2 and HEB 240 specimens in Mode 1, as indicated bellow.

The following analytical expressions for the deformation capacity of T-stubs for all three failure modes are proposed.

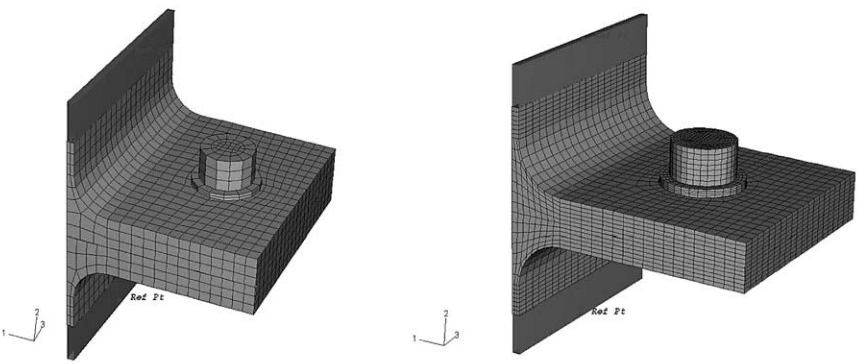

Mesh M4: Group 1 (HEB 200) Group 2 (HEA 260)

Fig. 12. Finite element meshing.

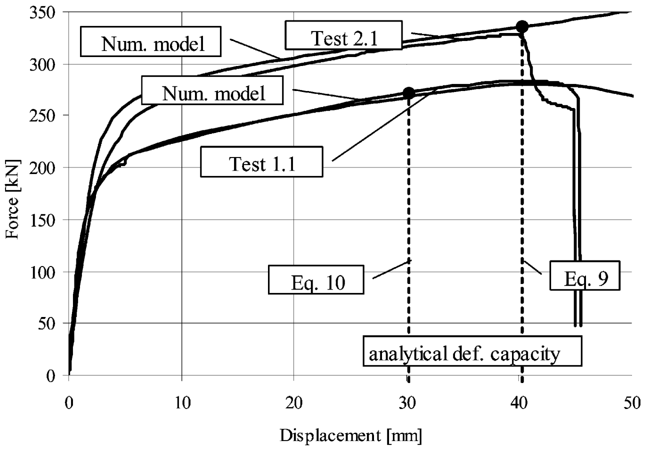

Fig. 13. Comparison of results—numerical analysis and test results.

2.5.1. *Mode 1 (complete yielding of the flange)*

The plastic mechanism of Mode 1 is presented in Fig. 14. Ultimate displacements, δ_u, can be calculated from:

$$\delta_u = \varphi \cdot m. \tag{9}$$

The rotation of the plastic hinge, φ, can be determined under the assumption that the maximum strain at the outer surface of the flange in bending, ε_u, cannot be larger than $\varepsilon_u = 0.20$, in order to prevent tearing of the material, and that the length of the plastic hinge l_p can be approximately set equal to the thickness of the flange t_f. Accordingly:

$$\varphi = \frac{\varepsilon_u \cdot l_p}{t_f/2} = \frac{\varepsilon_u \cdot t_f}{t_f/2} = 2 \cdot \varepsilon_u. \tag{10}$$

Deformation capacity δ_u is then:

$$\delta_u = 2 \cdot \varepsilon_u \cdot m = 0.4 \cdot m. \tag{11}$$

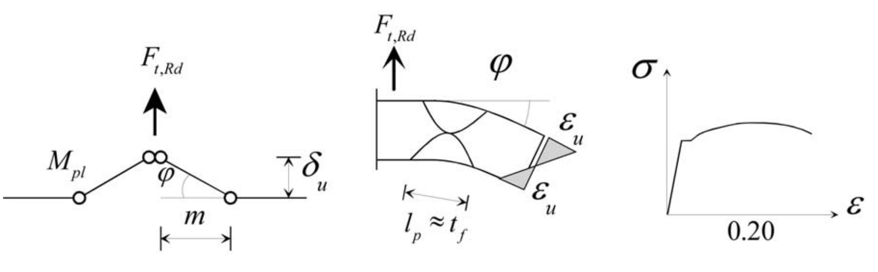

Fig. 14. Deformation capacity δ_u—Mode 1.

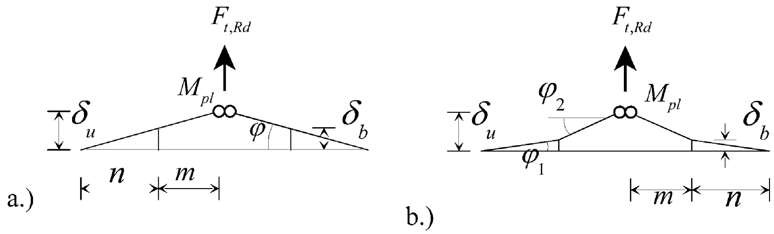

Fig. 15. Deformation capacity δ_u—Mode 2.

2.5.2. Mode 2 (bolt failure with yielding of the flange)

Mode 2 plastic mechanism according to prEN 1993-1-8 [1] is shown in Fig. 15a. It is used there in order to calculate the resistance of Mode 2. However, due to the local bending of flanges around bolts, the real deformation pattern is similar to the model in Fig. 15b. This kind of behaviour at ultimate loading was demonstrated in many tests (see also Fig. 11). The deformation capacity δ_u according to the model in Fig. 15b can be written as:

$$\delta_u = \varphi_1 \cdot n + \varphi_2 \cdot m. \tag{12}$$

φ_1 is obtained from the plastic deformation of bolts:

$$\varphi_1 = \frac{\varepsilon_{ub} \cdot l_b}{n} \tag{13}$$

where ε_{ub} is the maximum strain allowed in bolts, to prevent rupture of bolts in tension, which is set equal to 0.1. l_b is the clamping length of bolts, including the thickness of washers. φ_2 can be expressed in terms of φ_1 as

$$\varphi_2 = k \cdot \varphi_1 \tag{14}$$

where k is an empirical factor with values between 1.0 and 5.0. Hence, 1.0 is a very conservative value and 3.0–4.0 is the value that is normally reached.

Taking into account Eqs. 13 and 14, the final expression for δ_u is

$$\delta_u = 0.1 \cdot l_b \cdot \left(1 + k \cdot \frac{m}{n}\right). \tag{15}$$

2.5.3. Mode 3 (bolt failure)

The deformation capacity for this mode is simply the elongation of the bolts at failure:

$$\delta_u = \varepsilon_{ub} \cdot l_b = 0.1 \cdot l_b. \tag{16}$$

3. Determination of the rotation capacity of the entire joint

The characteristic moment–rotation curve as defined in prEN 1993-1-8 [1], is shown in Fig. 16, where φ_u is the rotation capacity. When the behaviour of compo-

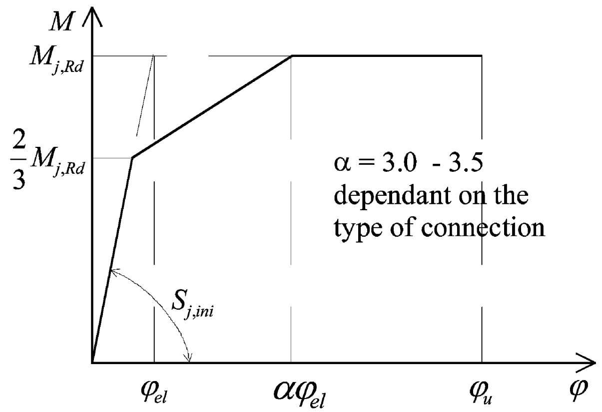

Fig. 16. Moment–rotation diagram from prEN1993-1-8.

nents, represented by bilinear diagrams (Fig. 3), is known, the rotation capacity of the whole joint may easily be obtained. A simple mechanical model for the joint behaviour composed of non-linear springs representing the relevant components (Fig. 17) can be established. The rotation capacity is primarily determined by the deformation capacity of the component with the lowest strength.

The main parameters that describe the behaviour of individual components are initial stiffness $\delta_{\mathrm{comp.ini}}$, strength $F_{\mathrm{comp.Rd}}$ and ultimate deformation capacity δ_{u} (Fig. 3). Section 2 describes how the deformation capacity can be determined, using simple analytical expressions. The initial stiffness and the strength can be obtained using prEN 1993-1-8.

In the overall deformation of the joint, the contributions of all individual components are included (Fig. 18). The component with the lowest strength contributes with its full deformation capacity, while the other components with the deformations at the stress level corresponding to that strength. It is therefore important to estimate the strength of each component as accurately as possible.

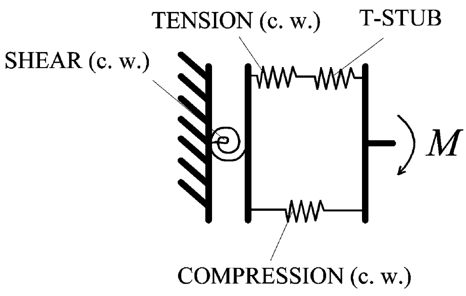

Fig. 17. Mechanical model of a joint.

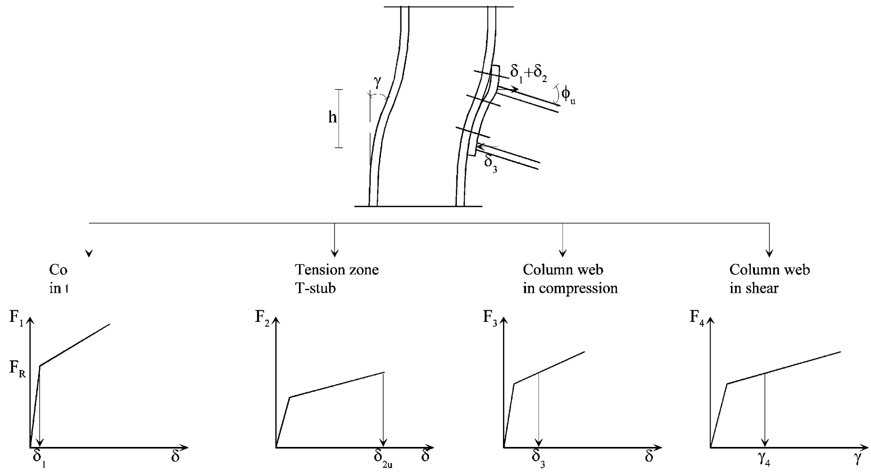

$$\phi_u = \frac{\delta_1 + \delta_2 + \delta_3}{h} + \gamma_4$$

Remarks:

1.) F_{2u} to be determined according to EC3, with 0.9 f_u (instead of f_y)

2.) The nonlinear branch of the curves starts, according to EC3, at 2/3 F_{iu}

Fig. 18. Flow chart for the determination of the rotation capacity of the joint.

Unfortunately, direct use of the strength, calculated according to prEN 1993-1-8, is not possible. The reason is that in prEN 1993-1-8 safe-sided expressions for the strength are provided, reflecting rather the strength at the onset of plasticity instead of the ultimate resistance, which is relevant for the deformation capacity. The problem can be overcome by using, in the design expressions of the code, the ultimate strength instead of yield stress when relevant (T-stub), and by using characteristic values of the strength parameters instead of the design values.

4. Comparison between analytical method and test results

The results of the proposed analytical method were compared to the test results of Bose et al. [21], who performed tests on joints with double-sided end-plate moment connections (Fig. 19). Four tests were selected for comparison (Table 1).

Because the rotation capacity is sensitive to the relative strength of individual components, four calculations of strength were performed with different values of material parameters (Cases 1–4):

- Case 1: Calculation strictly to prEN 1993-1-8

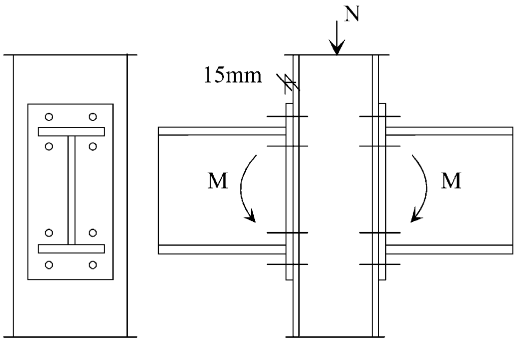

Fig. 19. Geometry of tested connections.

- Case 2: Measured f_y—all components, $\gamma_{M0} = 1.10$
- Case 3: Nominal f_y, for T-stub nominal f_u—without material safety factors
- Case 4: Measured f_y, for T-stub measured $0.9f_u$—without material safety factors

The last case is expected to be closest to real behaviour and can be regarded as characteristic resistance. Normally, measured values are not available and Case 3 can be regarded as relevant for the calculation of the rotation capacity.

The results of the comparison are given in Figs. 20–23, where moment–rotation diagrams are plotted, and in Table 2, where failure modes are compared.

It is evident that prEN 1993-1-8 [1] overestimates the initial stiffness and that the calculated strength is always lower than the measured one, irrespective of how strength parameters are taken into account.

Regarding the rotation capacity, there are significant differences in relation to the way of the determination of the strength. As expected, Case 4 gives the most accurate results that are safe, except for test No. 3, where a slight overestimation is observed.

Case 3 gives safe-sided results, but it is only for test No. 4 that the calculated rotation capacity is not too conservative. The reason for such unsatisfactory results, especially in comparison to test No. 3, are the measured values of yield stress and tensile strength that vary significantly from one component to another. In this case, nominal values do not represent the actual strength parameters satis-

Table 1
Geometry of tested connections

Test No.	Column	Beam	Bolts	Axial load in column (kN)
1	254 × 254 UC 89	457 × 191 UB 74	8 × M24 (8.8)	688
2	254 × 254 UC 89	762 × 267 UB 147		574
3	254 × 254 UC 73	457 × 191 UB 74		470
4	254 × 254 UC 132	457 × 191 UB 74		689

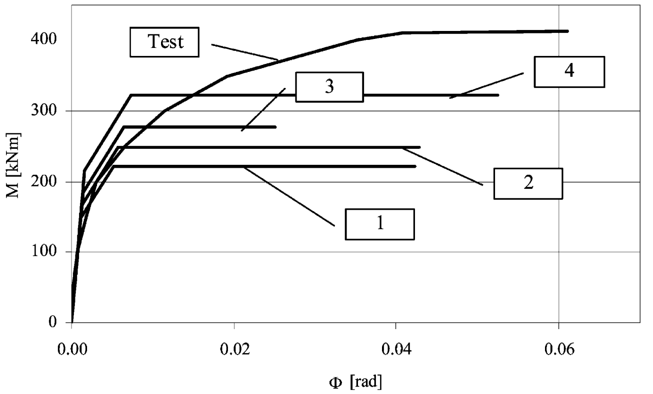

Fig. 20. Moment–rotation diagrams: Test No. 1 and analytical method.

factorily. It is worth mentioning that the same problem would occur with any other, even more elaborate, method, such as FE analysis. Inaccurate input cannot result in accurate results. It seems that the proper answer to this kind of difficulties could be a probabilistic approach.

For test No. 4 (Fig. 23), all cases give almost the same value of the rotation capacity. The reason is the very low end-plate resistance compared to the other components. This prevents other components from contributing to the rotation capacity. At the end of the test, bolt stripping—not accounted for in the analytical method—occurred and enlarged the measured value of the rotation capacity.

As stated above, the correct prediction of a failure mode, as well as the correct ratio of component resistances, is essential for an accurate prediction of the rotation capacity. In Table 2, failure modes are given for the test results and for

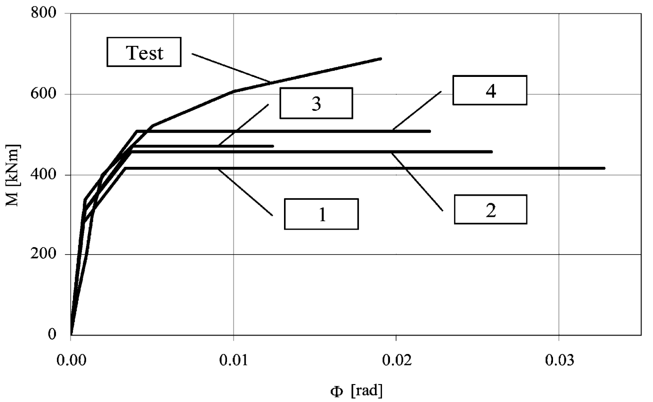

Fig. 21. Moment–rotation diagrams: Test No. 2 and analytical method.

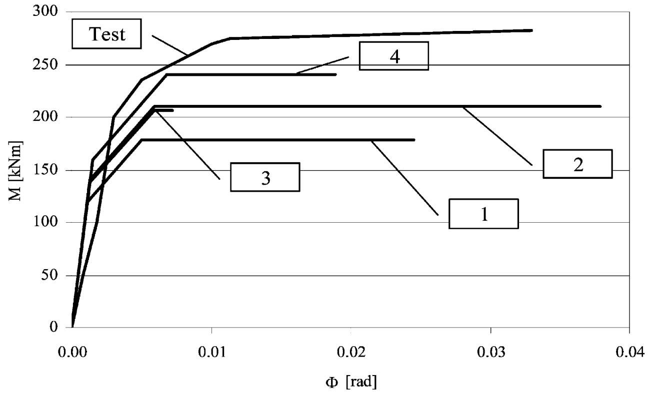

Fig. 22. Moment–rotation diagrams: Test No. 3 and analytical method.

the analytical method. Cases 3 and 4 were able to predict the correct failure mode for all four tests.

For test No. 3, the predicted rotation capacity for Cases 2 and 4 differs by a factor 2, although in both cases the correct failure mode, column web buckling, was detected.

These results can be explained by comparing load–displacement diagrams for an individual component (Fig. 24). In Case 2, the component web in compression has a small deformation capacity, but its strength is close to the strength of the end-plate and column flange. In this way, a relatively large deformation contribution from T-stub components is involved, resulting in a large rotation capacity. In Case 4, the strength of the column web in compression is lower and the other components contribute much less, resulting in a two times smaller rotation capacity than in Case 2.

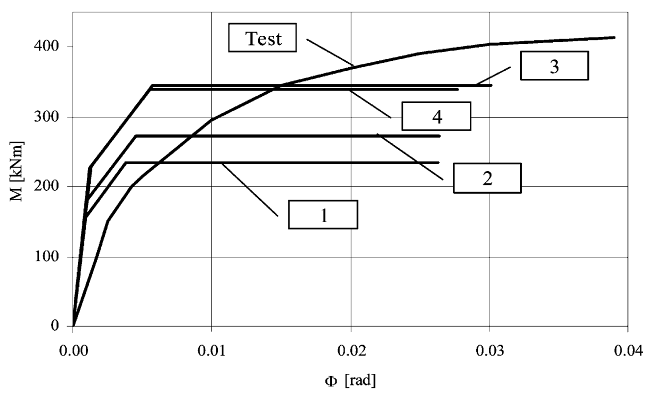

Fig. 23. Moment–rotation diagrams: Test No. 4 and analytical method.

Table 2
Failure modes

Case	Test No. 1	Test No. 2	Test No. 3	Test No. 4
Test	Column web buckling and end-plate fracture	Column web buckling	Column web buckling	Bolt fracture, bolt stripping and end-plate fracture
1	End-plate in bending 1. Row Mode 1 2. Row Mode 2	End-plate in bending 1. Row Mode 1 2. Row Mode 2	Column web in compression	End-plate in bending 1. Row Mode 1 2. Row Mode 2
2	End-plate in bending 1. Row Mode 1 2. Row Mode 2	Column web in compression	Column web in compression	End-plate in bending 1. Row Mode 1 2. Row Mode 2
3	Column web in compression	Column web in compression	Column web in compression	End-plate in bending 1. Row Mode 1 2. Row Mode 2
4	End-plate in bending 1. Row Mode 2 2. Row Mode 2	Column web in compression	Column web in compression	End-plate in bending 1. Row Mode 2 2. Row Mode 2

5. Conclusions

This paper presents a simple analytical method for the calculation of the rotation capacity of moment connections. An important feature of the method is its compatibility with the procedure given for the analysis of joints in prEN 1993-1-8 [1].

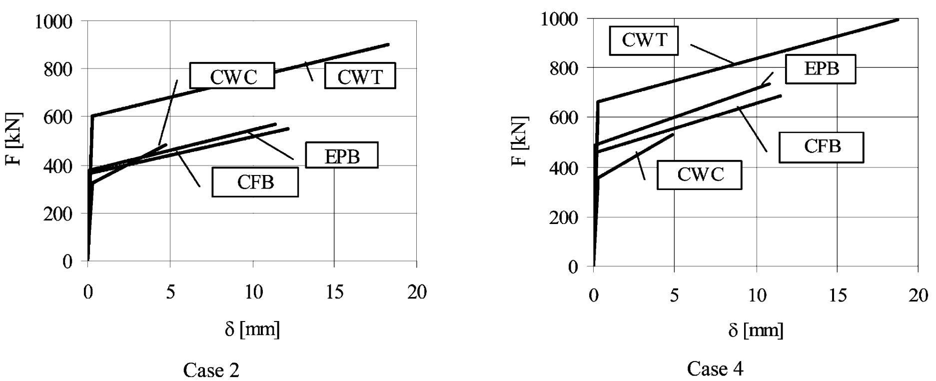

Fig. 24. Test No. 3: force–displacement diagram of components.

The proposed method gives simple numerical expressions for the deformation capacities of joint components, while the initial stiffness and strength of components can be assessed according to the above code.

A comparison with the test results shows good agreement and the calculated rotation capacity is lower than the measured values.

The relative strength of individual components is of great importance and it was shown that the characteristic values of the measured or at least of the nominal yield stress (column web) and ultimate strength (T-stub) should be used in the calculation of the rotation capacity instead of the design values of yield stress used in the code.

References

[1] Eurocode 3. Design of steel structures, Part 1.8. Design of joints. prEN 1993-1-8; 2000.

[2] Brown ND, Hughes AF, Anderson D. Prediction of initial stiffness of ductile end-plate steel connections. Proc Inst Civil Eng: Struct Build 2001;146:17–29.

[3] Foley CM, Vinnakota S. Toward design office moment–rotation curves for end-plate beam-to-column connections. J Construct Steel Res 1995;35:217–53.

[4] Bahaari MR, Sherbourne AN. Behavior of eight-bolt large capacity endplate connections. Comput Struct 2000;77:315–25.

[5] Coelho A, Bijlaard F, Silva L. On the deformation capacity of beam-to-column bolted connection. ECCS-T10, April 2002, Ljubljana.

[6] Bursi OS, Jaspart JP. Benchmarks for finite element modelling of bolted steel connections. J Construct Steel Res 1997;43:17–42.

[7] Bursi OS, Jaspart JP. Calibration of finite element model for isolated bolted end-plate steel connections. J Construct Steel Res 1997;44:225–62.

[8] Faella C, Piluso V, Rizzano G. Plastic deformation capacity of bolted T-stubs: theoretical analysis and testing. Moment resistant connections of steel frames in seismic area, design and reliability, RECOS. London: E&FN Spoon. 2000.

[9] Kuhlmann U, Kuhnemund F. Rotation capacity of steel joints. Verification Procedure and Component Tests, 2000.

[10] Bose B, Youngson GK, Wang ZM. An appraisal of the design rules in Eurocode 3 for bolted endplate joints by comparison with experimental results. Proc Inst Civil Eng: Struct Build 1996;116:221–34.

[11] Bose B, Sarkar S, Bahrami M. Extended endplate connections: comparison between three-dimensional nonlinear finite-element analysis and full-scale destructive tests. Struct Eng Rev 1996;8:315–28.

[12] da Silva L, Lima L, Vellasco P, Andrade S. Experimental behaviour of end-plate beam-to-column joints under bending and axial force. Database reporting and discussion of results. Report on ECCS-TC10 Meeting in Ljubljana, April. 2002.

[13] Zupančič E. Rotation capacity of semi rigid connections. Master of Science thesis, University of Ljubljana, April 2001.

[14] Sherbourne AN, Bahaari MR. 3D simulation of end-plate bolted connections. J Struct Eng 1994;120:3122–36.

[15] Sherbourne AN, Bahaari MR. simulation of bolted connections to unstiffened columns—I. T-stub connections. J Construct Steel Res 1996;40:169–87.

[16] Sherbourne AN, Bahaari MR. 3D simulation of bolted connections to unstiffened columns—II. Extended endplate connections. J Construct Steel Res 1996;40:189–223.

[17] Vayas I, Zupančič E, Beg D. Rotationskapazität von Knoten in Rahmen aus Stahl—Verformbarkeit der Komponenten. Bauingenieur 2003;78:44–52.

[18] Beg D, Zupančič E, Vayas I. On the rotation capacity of moment connections. Proceedings of the Third European Conference on Steel Structures, Eurosteel 2002, Coimbra, vol. II. 2002, p. 967–76.
[19] Gioncu V, Petcu D. Available rotation capacity of wide-flange beams and beam-columns, Part 1. Theoretical approaches. J Construct Steel Res 1997;43:161–217.
[20] Dubina D, Grecea D, Ciutina A, Stratan A. Influence of connection typology and loading asymmetry, RECOS: moment resistant connections of steel frames in seismic area, design and reliability, RECOS. London: E&FN Spoon. 2000.
[21] Bose B, Hughes AF. Verifying the performance of standard ductile connections for semi-continuous steel frames. Proc Inst Civil Eng: Struct Build 1995;110:441–57.